# Closed Form Current and Conductance Model for Symmetric Double-Gate MOSFETs using Field-dependent Mobility and Body Doping

V. Hariharan, R. Thakker, M. B. Patil, J. Vasi and V. Ramgopal Rao

Center for Nanoelectronics, Dept. of Electrical Engg., Indian Institute of Technology Bombay
Powai, Mumbai 400076, India. (Email: vharihar@ee.iitb.ac.in / rrao@ee.iitb.ac.in)

## ABSTRACT

A closed-form inversion charge-based long-channel drain current model is developed for a symmetrically driven, lightly doped Symmetric Double-Gate MOSFET (SDGFET). It is based on the drift-diffusion transport mechanism and considers velocity saturation using the Caughey-Thomas model with exponent *n=2*, vertical field mobility degradation and body doping. It is valid in sub-threshold as well as above-threshold. Its main feature is that the physical model for velocity saturation has been retained as an integral part of the model derivation, instead of adding its effect at the end by considering an averaged electric field. The model is also extended to model the Channel Length Modulation effect in the post-velocity saturation regime. Comparisons of currents and conductances are made with 2D device simulation results and a reasonable match is shown all the way from sub-threshold to strong inversion.

***Keywords***: double-gate, mosfet, field, mobility, doping

## 1 INTRODUCTION

Technology scaling of the conventional MOSFET is reaching a point where there are numerous problems with it going forward, and any suggested work-around has some other problem linked to it. As a result, alternate structures have been studied for quite a while. One such structure is the Double Gate MOSFET (DGFET), a practical realization of which is via the Double-Gate FinFET. DGFETs are more amenable to scaling compared to the conventional MOSFETs, by virtue of their better electrostatics [1, 2]. Also, as devices shrink, adjusting their threshold voltage by heavy doping in the channel is not an acceptable option because of problems like random dopant fluctuations and degraded channel mobility. Hence, it is of special interest to model lightly doped DGFETs. A DGFET with identical material and thickness for the front and back gate electrodes and dielectric, is called a symmetric DGFET (SDGFET).

There have been many efforts to model the drain current for DGFETs. References [3, 4] were based on charge-sheet-models. References [4-13] assumed a constant mobility. References [3, 14] considered velocity saturation effects using the Caughey-Thomas model or its variants with exponent *n=1* (the variants (eg. [15]) differing in the way the critical electric field $E_c$ relates to $v_{sat}$, but all of them nevertheless using an exponent *n=1*). References [16, 17] considered velocity saturation effects using an exponent *n=2* but they considered a *spatially averaged* lateral electric field as the driving field for velocity saturation. The key differentiator in the present work is that the velocity saturation effects are included as an integral part of the model derivation where the *spatial* variation of the lateral electric field driving the velocity saturation effect is represented accurately. Hence, the model is expected to be physically more accurate. Using an exponent *n=2* has been found to yield a better match with experimental data for N-channel devices [18]. Further, it has been suggested [19] that using an exponent *n=1* or any odd number for that matter, would yield a model that would fail the Gummel symmetry test at $V_{DS}=0$.

Our model also considers low-field mobility degradation and body doping. We describe next the high-level approach used in deriving the model, and we finally show a sampling of the final results in the form of $I_D$-$V_G$, $g_m$-$V_G$, $I_D$-$V_D$ and $g_{ds}$-$V_D$ plots showing analytical versus 2D device simulation results.

## 2 MODEL DERIVATION

The schematic of an ideal SDGFET is shown in Fig. 1.

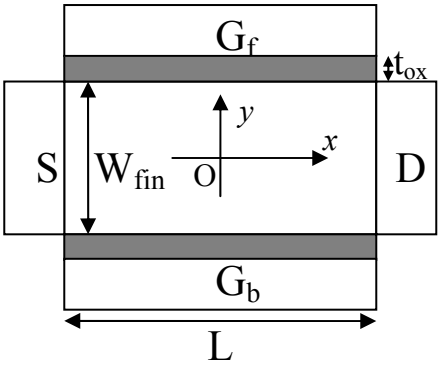


Fig. 1: Schematic of a SDGFET

Under the GCA and neglecting the body doping term initially, the 1D Poisson equation can be written as:

$$\frac{\partial^2 \psi}{\partial y^2} = \frac{q n_i}{\varepsilon} e^{(\psi - \phi_{fn})/\phi_t} \tag{1}$$

where $\psi$ is the electrostatic potential and $\varphi_{fn}$ is the electron quasi-fermi potential with respect to the $\varphi_{fn}$ value deep in the source end.

Proceeding as in [5], this can be solved to yield:

$$\frac{4\varepsilon\phi_t\beta_1\tan(\beta_1)}{W_{fin}C_{ox}}+\phi_{fn}+2\phi_t\ln\left(\frac{2\beta_1\sec(\beta_1)}{\beta W_{fin}}\right)-(V_{GS}-\Delta\phi)=f(\beta_1)=0 \quad (2)$$

where $\beta$ is given by:

$$\beta=\sqrt{\frac{qn_i}{2\varepsilon\phi_t}} \quad (3)$$

and $\beta_1$ is a state variable and is related to the inversion charge areal density:

$$Q_i=\frac{-8\varepsilon\phi_t\beta_1\tan(\beta_1)}{W_{fin}} \quad (4)$$

Now, in the drift-diffusion model, the drain current *per unit fin height* is:

$$I_{DS}=-\mu_{eff}(x)Q_i(x)\frac{d\phi_{fn}}{dx} \quad (5)$$

We describe next the approach adopted to incorporate the various physical effects.

## 2.1 Velocity Saturation

Velocity saturation is modeled using the Caughey-Thomas model [20] with exponent $n=2$:

$$\mu_{eff}(x)=\frac{\mu_0}{\sqrt{1+\frac{\mu_0{}^2E_{xs}{}^2}{v_{sat}{}^2}}} \quad (6)$$

In (6), we choose to model the driving field $E_x$ as being the lateral field at the *oxide-silicon interface* $E_{xs}$. This is not unreasonable, since even though charge sheet models are invalid in DGFETs [5] and there is non-negligible current flowing even far from the oxide-silicon interface, the current at the interface is still dominant (except in sub-threshold regime [21] where the leakiest path is along the fin center).

Proceeding then on the same lines as in [5], we finally get (7), where $\beta_2$ is given by (8). Equations (2) and (7) are the key equations that need to be solved. At this point, we make some very valid approximations, and derive a drain current model in terms of $\beta_{2s}$ and $\beta_{2d}$, where the suffixes $s$ and $d$ denote its values at the source and drain ends respectively.

$$\int_{\beta_{1s}}^{\beta_1}\left\{\frac{16\phi_t{}^2\beta_2{}^2}{I_{DS}{}^2}\left[\frac{2\varepsilon}{W_{fin}C_{ox}}\left(\beta_1\sec^2\beta_1+\tan\beta_1\right)+\frac{1+\beta_2}{\beta_1}\right]^2-\frac{\left(\beta_1\sec^2\beta_1+\tan\beta_1\right)^2}{C_{ox}{}^2v_{sat}{}^2}\right\}^{1/2}d\beta_1=\frac{-W_{fin}}{4\mu_0\varepsilon\phi_t}\left(x+\frac{L}{2}\right) \quad (7)$$

$$\beta_2=\beta_1\tan\beta_1 \quad (8)$$

As can be seen from (4), $\beta_2$ is proportional to the inversion charge areal density.

Again, making some approximations in (2) and (8), we bypass solving for $\beta_1$ and instead derive an approximate closed form solution for $\beta_2$ in terms of ($V_{GS}$ – $\varphi_{fn}$ – $\Delta\varphi$). Setting $\varphi_{fn}=0$ and $V_{DS}$ therein yields $\beta_{2s}$ and $\beta_{2d}$ respectively.

To calculate the drain saturation voltage $V_{DSat}$, we set $\partial I_{DS}/\partial V_{DS} = 0$, and make suitable approximations to get a closed form expression for $\beta_{2dsat}$. This results in a minimum $V_{GS}$ below which a $V_{DSat}$ does not exist (corresponding to the constraint that $\beta_{2d} > 0$, to be physically meaningful). We call this $V_{GS}$ as **VGSC**. This result is a direct consequence of considering drift as well as diffusion components in our approach. It is not possible to derive a closed-form exact expression for **VGSC**. So instead **VGSC** is deemed as a model parameter.

Having found $\beta_{2dsat}$ for a given $V_{GS}$, $V_{DSat}$ can be calculated using the approximated expressions discussed earlier.

To model channel-length-modulation (CLM) in the post-velocity saturation regime, we have used an approach similar to [22, 18] and modified it for a DGFET.

## 2.2 Body doping

Body doping is expected to be low in FinFETs and is therefore expected to make a difference only in the sub-threshold regime. We therefore solve the 1D Poisson equation in the sub-threshold regime, this time considering the body doping term. By comparing the expressions obtained with and without considering body doping, we then approximate a *merged* model for the electrostatic potential and electric field, such that they collapse to the correct respective expressions in the extreme cases of sub-threshold and above-threshold, and that they also collapse to the corresponding expressions in the extreme cases of

zero and non-zero body doping. The final result is the addition of a $N_a$ dependant spatially constant term in (2).

## 2.3 Low-field mobility degradation

To add support for vertical field mobility degradation in our core model, we use the same engineering model as that used in the PSP model [17], suitably modified for a DGFET for the depletion charge term, viz.

$$\mu_{eff} = \frac{\mu_0}{1+\left(\frac{|E_{eff}|}{E_0}\right)^{\theta} + \frac{CS}{\left(1+\frac{|\overline{Q_i}|}{qN_aW_{fin}}\right)^2}} \quad (9)$$

where:

$$|E_{eff}| = \frac{\eta|\overline{Q_i}| + qN_aW_{fin}}{2\varepsilon} \quad (10)$$

In doing so, we have introduced the following model parameters: $\mu_0$, $\theta$, $\eta$, $E_0$ and **CS**. The term $|avg(Q_i)|$ is a spatial average of $Q_i$ taken along the source-drain direction.

# 3 DEVICE SIMULATIONS

2D device simulations were done using Synopsis Sentaurus Device assuming abrupt source-body and drain-body junctions. In order to enable Coulomb scattering in the mobility calculation, the University of Bologna mobility model was used instead of the default Lombardi model. Simulations were done for 2 geometries, viz. *(i)* $L_g$=0.8um, $W_{fin}$=20nm, $T_{ox}$=1.4nm; and *(ii)* $L_g$=0.4um, $W_{fin}$=10nm, $T_{ox}$=1nm. For the 0.8um device, simulations were done for 4 different body dopings, viz. 1e16, 1e17, 1e18 and 2e18 $cm^{-3}$.

The device simulation results were used as virtual experimental data, and model parameters were extracted from it using a parameter extraction program developed at IIT Bombay [23] that is based on a stochastic method, viz. the Particle Swarm Optimization (PSO) algorithm.

# 4 PARAMETER EXTRACTION

The model has 16 parameters, of which 4 were set to known values (**WFIN**, **L**, **TOX** and **NA**) and the others were extracted in a 3-step fashion from $I_D$-$V_G$ (including $g_m$-$V_G$) and $I_D$-$V_D$ TCAD data.

In the first step, the work function difference **Δφ** was extracted from $I_D$-$V_G$ and $g_m$-$V_G$ data, limiting focus to $V_{DS}$=50mV and the sub-threshold regime ($V_{GS}$ < 0.4V). Reasonable default values were used for the other model parameters in this step.

In the second step, the low-field mobility degradation parameters were extracted from $I_D$-$V_G$ and $g_m$-$V_G$ data, considering the **Δφ** value extracted in the first step and giving it 5% freedom to vary in this step (called parameter refinement). This step continued to limit focus to $V_{DS}$=50mV but looked at the entire range of $V_{GS}$.

In the third step, the velocity saturation and CLM parameters were extracted from $I_D$-$V_D$ data considering the parameters extracted up until the prior steps. However the low-field mobility parameters were refined by up to 3% in this step. This step focused on $I_D$-$V_D$ data for $V_{GS}$ >= 0.5V.

The **VGSC** parameter was extracted in all 3 steps, though it makes its presence felt only in the third step. It is extracted in the first two steps in order to avoid complex number evaluations in those steps (which could happen in the $V_{DSat}$ expressions, if an appropriate default value for it is not chosen).

# 5 RESULTS

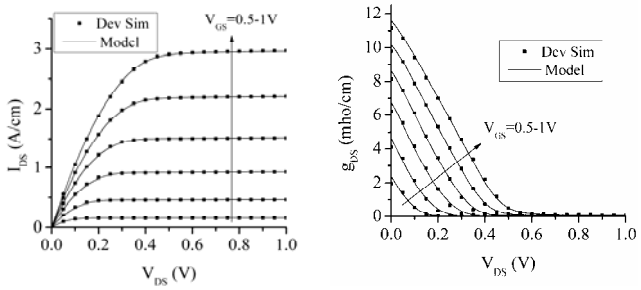


Fig. 2: $I_d$-$V_d$ (left) and $g_{ds}$-$V_d$ (right) for the 0.8um device with 1e15 body doping

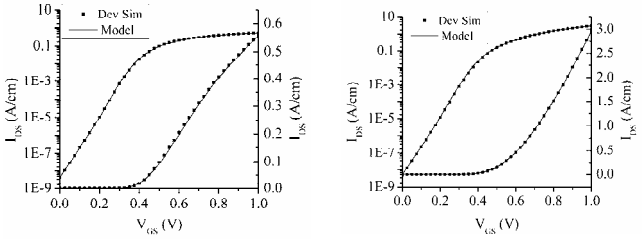


Fig. 3: $I_d$-$V_g$ @ $V_d$=50mV (left) and 1V (right) for the 0.8um device with 1e15 body doping

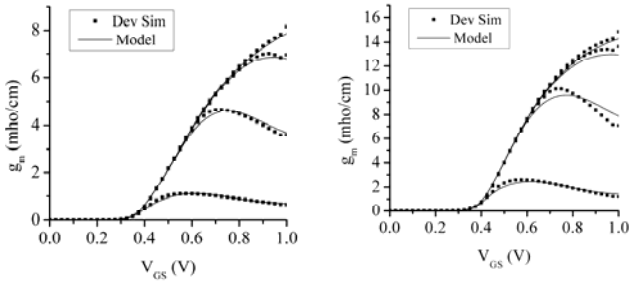


Fig. 4: $g_m$-$V_g$ for the 0.8um (left) and 0.4um (right) device with 1e15 body doping, for $V_d$=50mV, 0.24V, 0.43V and 1V

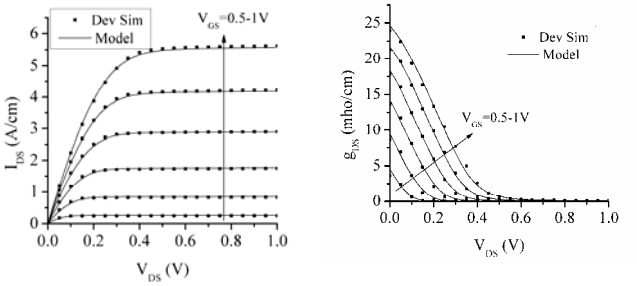


Fig. 5: $I_d$-$V_d$ (left) and $g_{ds}$-$V_d$ (right) for the 0.4um device with 1e15 body doping

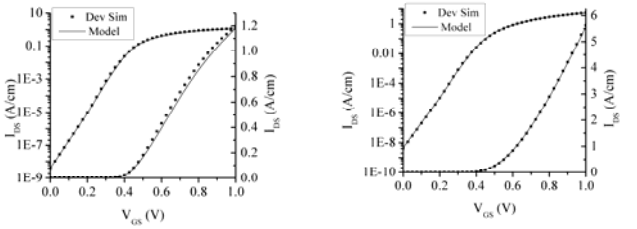


Fig. 6: $I_d$-$V_g$ @ $V_d$=50mV (left) and 1V (right) for the 0.4um device with 1e15 body doping

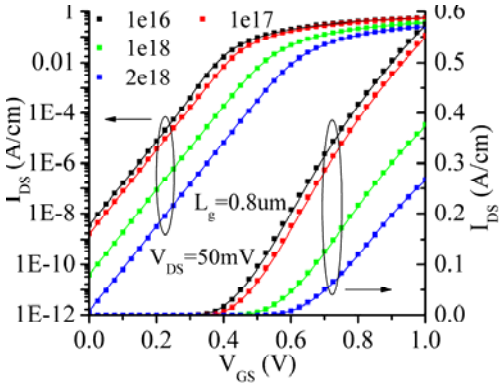


Fig. 7: $I_d$-$V_g$ for various body dopings. The dots are device simulation data, the lines of the corresponding color are model data

Fig. 2-6 show a sampling of various $I_D$-$V_D$, $g_{ds}$-$V_D$, $I_D$-$V_G$ and $g_m$-$V_G$ curves showing analytical versus device simulation results. Fig. 7 shows the analytical versus device-simulation $I_D$-$V_G$ curves for various body dopings. All quantities are shown per unit fin height. As can be seen, the match is very good.

## 6 CONCLUSIONS

A closed-form inversion charge-based long-channel drain current model has been developed for a symmetrically driven, lightly doped Symmetric Double-Gate MOSFET (SDGFET), considering field-dependent mobility and body doping.

## ACKNOWLEDGMENT

This work was performed at the Centre of Excellence for Nanoelectronics (CEN), IIT Bombay, which is supported by the Ministry of Communications & Information Technology, Govt. of India. Synopsys Inc. is also gratefully acknowledged for their TCAD tool support.

## REFERENCES

[1] P. M. Solomon et al., *IEEE CDM*, pp. 48-62, Jan 2003.
[2] E. J. Nowak et al., *IEEE CDM*, pp. 20-31, Jan/Feb. 2004.
[3] G. Pei, W. Ni, A. V. Kammula, B. A. Minch, and E. C-C. Kan, *IEEE TED*, vol. 50, pp. 2135-2143, Oct. 2003.
[4] M. V. Dunga et al., *IEEE TED*, vol. 53, pp. 1971-1978, Sep. 2006.
[5] Y. Taur, X. Liang, W. Wang, and H. Lu, *IEEE EDL*, vol. 25, pp. 107-109, Feb. 2004.
[6] Jin He et al., *Proc. ISQED*, p. 45, 2004.
[7] J. M. Sallese et al., *SSE*, vol. 49, pp. 485-489, Mar. 2005.
[8] A. S. Roy, J. M. Sallese, C.C. Enz, *SSE*, vol. 50, pp. 687-693, Apr. 2006.
[9] H. Lu and Y. Taur, *IEEE TED*, vol. 53, pp. 1161-1168, May. 2006.
[10] A. Ortiz-Conde, F. J. G. Sanchez, J. Muci, *SSE*, vol. 49, pp. 640-647, Apr. 2005.
[11] Jin He et al., *IEEE TED*, vol. 54, pp. 1203-1209, May 2007.
[12] Z. Zhu et al., *Elec. Lett.*, vol. 43, pp. 1464-1466, Dec. 2007.
[13] Z. Zhu, X. Zhou, K. Chandrasekaran, S. C. Rustagi, and G. H. See, *JJAP*, vol. 46, No. 4B, 2007, pp. 2067-2072.
[14] M. Wong and X. Shi, *IEEE TED*, vol. 53, pp. 1389-1397, Jun. 2006.
[15] C. G. Sodini, Ping-Keung Ko and J. L. Moll, *IEEE TED*, vol. 31, pp. 1386 – 1393, Oct. 1984.
[16] G. D. J. Smit et al., *NSTI-Nanotech*, vol. 3, pp. 520-525, 2007.
[17] G. Gildenblat, et al., *IEEE TED*, vol. 53, pp. 1979-1993, Sep. 2006.
[18] Y. Taur and T. Ning, *Fundamentals of Modern VLSI Devices*, Cambridge Univ. Press, 2003.
[19] K. Joardar, K. K. Gullapalli, C. C. McAndrew, M. E. Burnham, and A. Wild, *IEEE TED*, vol. 45, pp. 134-148, Jan. 1998.
[20] D. M. Caughey and R. E. Thomas, *Proc. IEEE*, vol. 55, pp. 2192 - 2193, Dec. 1967.
[21] G. Pei, J. Kedzierski, P. Oldiges, M. Ieong, and E. C-C. Kan, *IEEE TED*, vol. 49, pp. 1411-1419, Aug. 2002.
[22] P. K. Ko, et al, *IEDM*, pp. 600-603, 1981.
[23] R. Thakker, N. Gandhi, M. Patil, and K. Anil, *IWPSD*, pp. 130-133, 2007.